Chemical Engineering Journal 448 (2022) 137637

Contents lists available at ScienceDirect

Chemical Engineering Journal

journal homepage: www.elsevier.com/locate/cej

Janus hydrogel-based fuel stimulant powered amplification for multiple detections of miRNA biomarkers in gastric cancer

Jaewoo Lim [a,c,1], Jin-Seong Hwang [b,d,1], Seung Beom Seo [a,e], Byunghoon Kang [a], Soojin Jang [a,c], Seong Uk Son [a,c], Jisun Ki [a], Jang-Seong Kim [b,d], Taejoon Kang [a], Juyeon Jung [a,c], Tae-Su Han [b,d,*], Eun-Kyung Lim [a,c,*]

[a] Bionanotechnology Research Center, Korea Research Institute of Bioscience and Biotechnology (KRIBB), 125 Gwahak-ro, Yuseong-gu, Daejeon 34141, Republic of Korea
[b] Biotherapeutics Translational Research Center, Korea Research Institute of Bioscience and Biotechnology (KRIBB), 125 Gwahak-ro, Yuseong-gu, Daejeon 34141, Republic of Korea
[c] Department of Nanobiotechnology, KRIBB School of Biotechnology, University of Science and Technology, 125 Gwahak-ro, Yuseong-gu, Daejeon 34113, Republic of Korea
[d] Department of Functional Genomics, KRIBB School of Bioscience, University of Science and Technology, 125 Gwahak-ro, Yuseong-gu, Daejeon 34113, Republic of Korea
[e] Department of Cogno-Mechatronics Engineering, Pusan National University, 2 Busandaehak-ro 63beon-gil, Geumjeong-gu, Busan 46241, Republic of Korea

ARTICLE INFO

Keywords:
Gastric cancer
Cancer diagnosis
microRNA
Janus hydrogel
Fuel stimulant-powered amplification

ABSTRACT

MicroRNAs (miRNAs) circulating in body fluid have emerged as potential biomarkers for various diseases; however, owing to their low concentrations and short lengths (~22 nt), their clinical applications are still limited. Therefore, a highly sensitive and selective novel diagnostic platform for miRNA detection is required. Here, we present a hydrogel-based fuel stimulant-powered (FSP) amplification of fluorescent signals to detect circulating miRNAs from clinical samples of human serum. The advantage of this method is that it has high sensitivity as a fuel-assisted DNA cascade reaction that does not require temperature control and enzymes used for nucleic acid amplification. Further, we developed a Janus-type hydrogel for the simultaneous detection of the gastric cancer-associated miRNAs, miR-135b and miR-21. The detection limit of this hydrogel-based FSP amplification using synthetic miRNAs was estimated as < 10 fmol. We also validated the performance of this amplification process in *in vitro* and in vivo models and clinical samples. Therefore, we demonstrate that Janus hydrogel-based FSP amplification can selectively and sensitively identify the overexpression of miR-135b and miR-21 in clinical samples, thereby helping distinguish gastric cancer patients from healthy donors.

1. Introduction

Gastric cancer (GC) is globally the fifth most frequently diagnosed cancer (1,089,103 new cases in 2020) and the fourth leading cause of cancer-related death (768,793 deaths) among all malignancies [1,2]. Carcinoembryonic antigen and carbohydrate antigens (*e.g.,* CA19-9, CA72-4) have been commonly used for the early clinical detection of GC [3–6]. However, these serum biomarkers have poor specificities and are not unique GC markers [7,8]. Therefore, developing an improved diagnostic method for early GC remains a significant challenge. In the last decade, epigenetic alternations (such as DNA methylation and histone modification), long non-coding RNAs, and microRNAs (miRNAs)

Abbreviations: GC, Gastric cancer; miRNA, microRNA; qRT-PCR, quantitative real time-reverse transcription polymerase chain reaction; FSP, fuel stimulant-powered; D1, DNA 1 sequence; D2, DNA 2 sequence; FSP-135b, FSP probe specific for miR-135b, FAM, fluorescein phosphoramidite; BHQ1, black hole quencher 1; FSP-21, FSP probe specific for miR-21; Cy3, cyanine 3; BHQ2, black hold quencher 2; PAGE, polyacrylamide gel electrophoresis; PDMS, polydimethylsiloxane; UV, ultraviolet; F.I., fluorescence intensity; LOD, limit of detection; PEG, poly(ethylene glycol); DIPEA, *N,N*-diisopropylethylamine; DCM, dichloromethane; HMPP, 2-hydroxy-2-methylpropiophenone; TBE, Tris-Borate-EDTA; TE, Tris-EDTA; DMEM, Dulbecco′s Modified Eagle′s Medium; FBS, fetal bovine serum; P/S, penicillin-streptomycin; PEGDA, polyethylene glycol diacrylate.

* Corresponding authors.
E-mail addresses: tshan@kribb.re.kr (T.-S. Han), eklim1112@kribb.re.kr (E.-K. Lim).
[1] Jaewoo Lim and Jin-Seong Hwang contributed equally to this work.

https://doi.org/10.1016/j.cej.2022.137637
Received 8 March 2022; Received in revised form 23 May 2022; Accepted 16 June 2022
Available online 18 June 2022

have been spotlighted as potential biomarkers to overcome this challenge [9].

Notably, miRNAs are small (~22 nt) non-coding RNAs that regulate gene expression [10,11] and are essential modulators of various diseases, including GC [12–16]. Aberrant overexpression or downregulation of miRNAs can be oncogenic and/or tumor suppressing depending on the function of the target gene [17–19]. Interestingly, cell-free circulating miRNAs secreted by tumors, including exosomal miRNAs, are potential GC-associated biomarkers for non-invasive liquid biopsies [20–23]. Moreover, the most widely used techniques for profiling miRNAs in cancer are microarray-based approaches [24–26] and quantitative real time-reverse transcription polymerase chain reaction (qRT-PCR) [27]. However, these techniques are limiting, as they are costly, sophisticated, labor-intensive, and time consuming processes [28–31]. In the last decade, novel diagnostic tools using the cascade DNA strand displacement techniques have been announced, and it is expected to be able to replace the conventional method [32–33].

Hydrogel-based sensors have emerged as promising biomedical platforms because of their low fabrication costs [34] and high detection capacities owing to their 3D structures [35]. Additionally, since they are made of non-fouling materials, they have significantly enhanced specificities and sensitivities [36] and have negligible background colors and fluorescence emissions [37]. Nevertheless, these sensors are still insufficient in detecting low concentrations of miRNAs in body fluids.

Here, we have developed Janus hydrogel-based fuel stimulant-powered (FSP) amplification for the detection of miRNAs circulating in body fluids. We designed a signal amplification strategy using a fuel-assisted DNA cascade reaction and integrated this concept with hydrogels [38,39]. Since signal amplification in this method is independent of enzymes or temperature control, this method is highly sensitive and advantageous. Based on previous reports, we tested our diagnostic platform by attempting to detect miR-135b [40], which is involved in carcinogenesis and the development of gastric inflammation, and miR-21, a well-known oncogene [41–43]. We also validated the potential of the Janus hydrogel-based FSP amplification platform in detecting gastric cancer in clinical samples (15 healthy controls, 15 GC patients with stage I-II, and 15 GC patients with stage III-IV) by comparing it to the widely used qRT-PCR. Our study demonstrates that the proposed novel platform is a simple but robust diagnostic tool for early cancer detection and prognosis monitoring through quantitative analysis of gastric cancer-associated miRNA.

2. Materials and methods

2.1. Reagents, materials, cell lines, and animals

We purchased poly(ethylene glycol) (Mn 3,350; PEG 3.35 K), *N,N*-diisopropylethylamine (DIPEA), dichloromethane (DCM), and the radical photo-initiator 2-hydroxy-2-methylpropiophenone (HMPP) from Sigma-Aldrich (USA). Additionally, we purchased acryloyl chloride from Tokyo Chemical Industry Co. (Japan) and 10 × Tris-Borate-EDTA (TBE) buffer and 1 × Tris-EDTA (TE) buffer from Biosesang (Korea). Poly(dimethylsiloxane) Sylgard 184 and SU-8 negative photoresist and SU-8 developer were purchased from Dow Corning and Microchem (Japan), respectively. Acrylamide/bis-acrylamide solution (19:1, 40%), tetramethylethylenediamine, and ammonium persulfate were purchased from Bio-Rad Lab., Inc. (USA). Furthermore, RPMI-1640 medium, Dulbecco′s Modified Eagle′s Medium (DMEM), fetal bovine serum (FBS), 100 × penicillin–streptomycin (P/S), and Ultra-low range DNA ladder were purchased from Thermo Fisher Scientific Inc (USA). Exospin™ kit was purchased from Cell Guidance Systems (UK), whereas ExoRNeasy Maxi kit, RNeasy Mini Kit, miScript II RT Kit, and miScript SYBR Green PCR Kit were purchased from Qiagen (Germany). All oligonucleotides were purchased from Bioneer Co. (Korea) and were purified by high-performance liquid chromatography and dissolved in the TE buffer.

2.2. Cell culture

We obtained the human gastric cancer cell lines SNU601 (CVCL_0101), SNU638 (CVCL_0102), KATO III (CVCL_0371), NCI-N87 (CVCL_1603), and MKN-45 (CVCL_0434) from the Korean Cell Line Bank (Republic of Korea). These cell lines were cultured in RPMI-1640 medium supplemented with 10% FBS and 1 × P/S. The mouse fibroblast cell line NIH3T3 (ATCC® CCL-92™) was purchased from American Type Culture Collection (USA) and was cultured in DMEM containing 10% FBS and 1 × P/S.

2.3. Establishment of an in vitro model

We established an miRNA-135b-expressing cell line, as described previously [38]. First, we amplified and cloned the full-length coding region of miRNA-135b cDNA into the pmR-ZsGreen1 vector (Takara Bio Inc.). The following primers were used for the cloning: 5′-CCGC TCGA GTTT ATGG CCAG GAAG-3′ (forward) and 5′-CGGG ATCC AAGG TCTC CTTC CTT-3′ (reverse). Subsequently, we selected miRNA-135b-expressing cells by adding 500 μg/mL (final concentration) of geneticin (Thermo Fisher Scientific) to the medium. Eventually, green fluorescence protein-positive cells were sorted using a fluorescence-activated cell sorter (Thermo Fisher Scientific, Waltham, MA, USA).

2.4. Establishment of a xenograft mouse model

To establish a xenograft mouse model, we first subcutaneously injected the right flank of 5-weeks-old female Balb/c-nu mice (Orientibio, Seongnam, Korea) with empty vector-transfected (SNU638_control) or stable miRNA-135b-overexpressing SNU-638 cells (SNU638_over). The miRNA expression levels in the xenograft mice sera were then compared with that in the normal mice sera ($n = 5$). Furthermore, we measured the tumor size twice a week using calipers and calculated the tumor volume using the following formula: volume = length × width^2, wherein length is defined as the longest diameter and width is defined as half of the diameter that is perpendicular to the length. Sera and tumor tissues were collected from the mice models for subsequent analysis. The animal experiments were approved by the Committee on Animal Experimentation of the Korea Research Institute of Bioscience and Biotechnology (approval No. KRIBB-AEC-21130).

2.5. Acquisition of clinical human serum samples

This study was approved by the Institutional Review Board from Biobank of Ajou University Hospital and Korea Research Institute of Bioscience and Biotechnology (approval No. AJHB-2021–20 and P01-202105–31-011). In this study, we collected samples from patients clinically diagnosed with GC based on the American Joint Committee on Cancer (AJCC) staging manual. This manual contains standard classifications for tumor, lymph node, and metastasis staging systems. We collected human serum samples belonged to healthy controls ($n = 15$) and patients with stages I–II of GC ($n = 15$) and those with stages III–IV of GC ($n = 15$). The serum biospecimens were provided by the Biobank of Ajou University Hospital (Korea).

2.6. Extraction of total RNA

We isolated exosomes from human and mouse serum samples using ExoQuick™ (System Biosciences, Palo Alto, CA, USA) and those from the cell culture medium using ExoQuic-TC™ (System Biosciences), as per the manufacturers' instructions. Thereafter, we extracted exosomal RNA using the RNeasy Micro kit (Qiagen) and isolated total RNA from mammalian cells and mouse tumor tissues using Nucleozol (Macherey-Nagel Co.).

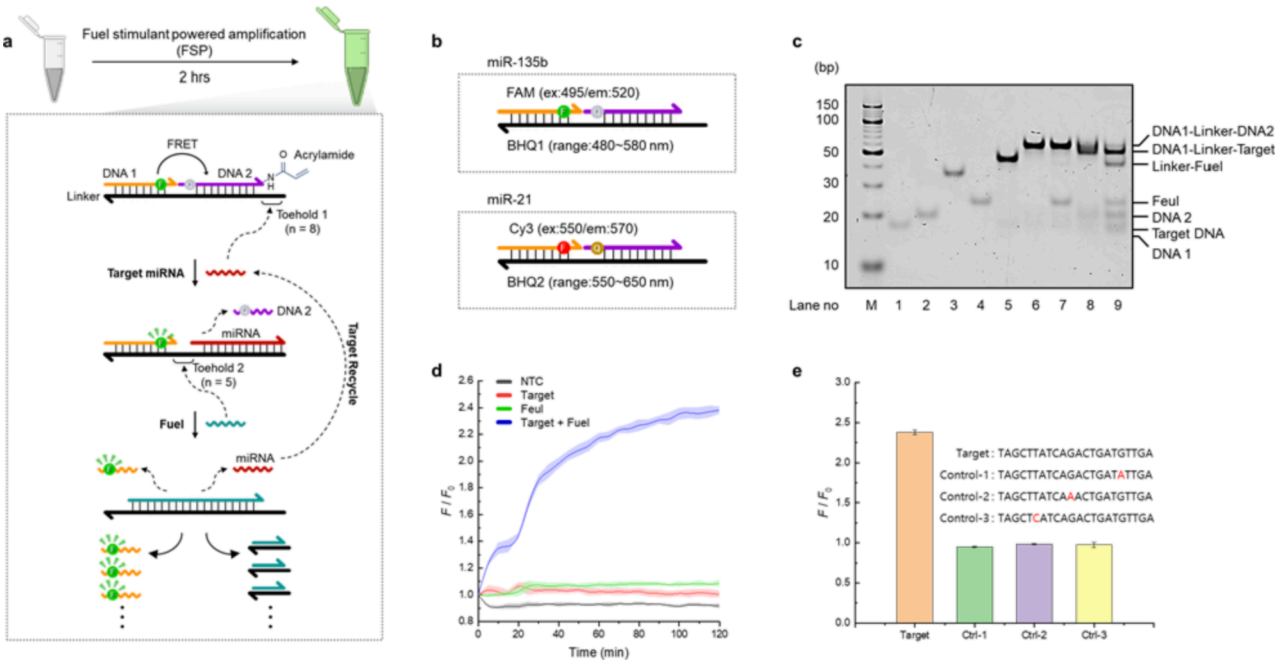

Fig. 1. Programming of the fluorescence signal amplification strategy. a) Schematic illustration of the fuel stimulant-powered (FSP) amplification for miRNA detection. Target miRNAs triggered fluorescence signal recovery *via* toehold 1-mediated strand displacement. The fuel then combines with the linker DNA *via* the toehold 2-mediated strand displacement. These reactions induce signal amplification by target recycling. The FSP probe ligates to the hydrogel *via* the acylamide-tagged 3′ end of DNA 2. b) The FSP probe is designed to detect miR-135b and miR-21. FSP-135b contains fluorescein phosphoramidite (FAM) and black hole quencher 1 (BHQ1) tagged to the 3′ of DNA 1 and 5′ end of DNA 2, respectively. FSP-21 contains Cyanine 3 (Cy3) and black hole quencher 2 (BHQ2) tagged to the 3′ of DNA 1 and 5′ end of DNA 2, respectively. c) Polyacrylamide gel electrophoretic analysis of the FSP amplification products. M: marker, lane 1: DNA 1 (D1), lane 2: DNA 2 (D2), lane 3: linker DNA (L), lane 4: fuel (F), lane 5: D1-L, lane 6: FSP (D1-L-D2), lane 7: FSP-F, lane 8: FSP-target (T), lane 9: FSP-F-T. d) Fluorescence recovery (F/F_0) measurement of FSP probe solution containing 10 nM target, 100 nM fuel, and both. e) Fluorescence recovery measurement of the FSP probes conjugated with the target and single mismatched controls. These control DNAs had a random nucleotide changed from that of the target sequence.

2.7. Quantitative real-time PCR

We assessed RNA quantity using Nanodrop™ 2000 (Thermo Scientific). Subsequently, we performed first-strand cDNA synthesis from equal amounts of each sample using the miScript II RT Kit (Qiagen). Additionally, qRT-PCR reactions were conducted on a CFX96™ Real-Time PCR System (Bio-Rad), in accordance with the protocol provided with the miScript SYBR Green PCR Kit. Expression levels of different miRNAs were normalized to that of RNU6B [44,45].

2.8. Synthesis of polyethylene glycol diacrylate

We synthesized a hydrogel backbone made from polyethylene glycol diacrylate (PEGDA) as described previously [46,47]. In this regard, we first completely dissolved 60 g of PEG (molecular weight: 3,400 Da) in 75 mL of DCM. Once this solution became transparent, we added 7 mL of DIPEA to it. Following this, we added 6.5 mL of acryloyl chloride to the solution dropwise while stirring it vigorously on ice, i.e. at 4 ℃; this mixture was stirred overnight in the dark and in a nitrogen-containing atmosphere. Subsequently, this reactant was precipitated in 1 L of diethyl ether and filtered; the filtrate was vacuum dried to obtain a powder. We eliminate any by-products by dissolving this powder in 75 mL of DCM and 500 mL of 2 M potassium carbonate (K_2CO_3) and subjecting the solution to an overnight phase separation. A lower layer of organic solution was filtered and precipitated in 1 L of diethyl ether and was dried under vacuum. This synthesized PEGDA was stored at 4 ℃ until further use.

2.9. Fabrication of a hydrogel-based fuel stimulant

We developed cylindrical hydrogels by photo-polymerization of PEGDA. While the master template with vertical column patterns was manufactured by 3D printing, the hydrogel mold was constructed *via* soft lithography using the master template and PDMS. A PDMS mixture containing a base and curing agent (10:1 wt ratio) was poured over the master template and heated at 80 °C for 6 h (**Figure S3**). Subsequently, we poured 15 μL of a hydrogel precursor solution (20% [w/v] PEGDA, 20% [w/v] PEG, 60% [v/v] 1 × TE buffer, and 0.1% [v/v] HMPP) onto the hydrogel mold. Subsequently, we performed photo-polymerization for 2 min using a 254 nm UV lamp. The fabricated cylindrical hydrogels were rinsed in distilled water for 1 h and stored at 4 ℃ until further use. Next, we fabricated the Janus hydrogels in two steps (Fig. 3a). First, we poured 15 μL of the hydrogel precursor solution into the half-patterned hydrogel mold made from PDMS. Thereafter, we performed photo-polymerization for 2 min using a UV lamp (254 nm). The pair of unrinsed, cured hydrogels were then cast within a round frame (Acrylonitrile Butadiene Styrene, ABS) and were subjected to additional UV irradiation to bind them. Eventually, the fabricated Janus hydrogels were rinsed in distilled water for 1 h.

2.10. Hydrogel-based FSP signal amplification

We performed the signal amplification using FSP probes consisting of fluorescence-labeled DNA 1 (FAM or Cy3), quencher-tagged DNA 2 (BHQ1 or BHQ2), and a linker DNA; their sequences are listed in Table S1. Notably, these probes fixed to the hydrogel *via* the 3́-acylamide group of DNA 2 (Fig. 1a). The concentration of 3.33 μM DNA 1, DNA 2, and the linker DNA were annealed at 90 ℃ for 5 min and cooled down slowly to 25 ℃. We mixed 0.5 μM of the FSP probes with hydrogel precursor solution, and subsequently cured 15 μL of the precursor solution in a cylindrical or half-patterned hydrogel mold. Non-crosslinked probes or hydrogel polymers were eliminated in the washing step. Thereafter, we added 100 ng of either the extracted total RNA (including, *in vitro*, in vivo, and clinical samples) or varying synthetic

miRNA concentrations into 1 × TAE buffer (containing 12.5 μM of $MgCl_2$). To this solution we then added 0.5 μM of fuel DNA (F). A final volume of 20 μL of the sample solution was then added to the cylindrical hydrogel and incubated for 2 h at 25 ℃. In contrast, 50 μL of a sample solution containing two types of fuel DNA (miR-21 and miR-135b) was added to the Janus hydrogels. Eventually, we acquired and analyzed the fluorescence emitted by the hydrogels using a gel imaging system (Bio-Rad Laboratories, USA). The analytical performances of Janus hydrogel were summarized in Table S2.

2.11. Fluorescence measurement

We designated the following fixed gain when measuring the fluorescence intensities of the FSP probes in the sample solutions: $\lambda_{ex} = 484$ nm and $\lambda_{em} = 530$ nm. The intensities were assessed using a Cytation 5 plate reader (BioTek). In this regard, we measured the increase in fluorescence intensities of the probes before and after addition of the target gene sequences to the sample (F / F_0).

2.12. Electrophoresis analysis

We validated the reaction of the FSP fluorescence signal amplification by conducting a PAGE. First, we loaded the oligonucleotides that serially reacted in each step on the gel. Subsequently, this gel was run in a 10% acrylamide solution containing 1 × TBE buffer under a constant voltage (80 V) for 1.5 h at room temperature. Subsequently, we stained the gel with a nucleic acid-staining dye (Gel-Red) for 10 min and observed it under a gel imaging system (Bio-Rad Laboratories, USA) to visually confirm that the FSP reaction did occur.

2.13. Statistical analysis of obtained data

All experiments were conducted independently at least thrice; the exact number of replicates is mentioned in each graph. Data have been reported as mean ± standard deviation. The following legend has been added to each figure: *p-value < 0.05; **p-value < 0.005; and ***p-value < 0.00005. LOD was calculated by the following equation: LOD = 3σ / m, where σ is the standard deviation of the blank sample and m is the slope of the data fitted in a linear range.

3. Results and discussion

3.1. Programming of the fluorescence signal amplification strategy

Fig. 1a depicts the FSP signal amplification strategy that we designed to detect low concentrations of circulating miRNAs in a sample. The FSP probe complex consisted of a fluorophore-tagged DNA 1 sequence (D1), quencher and acylamide-tagged DNA 2 sequence (D2), and linker DNA. We designed the probe such that the linker DNA had eight toehold sequences (toehold 1) for binding to the target miRNAs. In the presence of a target sequence, D2 of the FSP probe was replaced with the target sequence, thereby recovering the fluorescence signal. Once D2 was separated, five of the toehold sequences (toehold 2) became open and induced complementary binding between the linker and the fuel. Consequently, the target sequence was separated from the linker and subsequently bound to another FSP probe complex. This reaction continued until the fuel was exhausted. In this study, we prepared two FSP probes for the simultaneous detection of miR-135b, and miR-21 (Fig. 1b). The FSP probe specific for miR-135b (FSP-135b) was tagged to fluorescein phosphoramidite (FAM) and black hole quencher 1 (BHQ1). In contrast, the FSP probe specific for miR-21 (FSP-21) was tagged to cyanine 3 (Cy3) and black hold quencher 2 (BHQ2). The sequences of these FSP probes are listed in Table S1. Subsequently, we analyzed the FSP amplified products *via* polyacrylamide gel electrophoresis (PAGE; Fig. 1c). The resultant gel images demonstrated that the D1, D2, and linker sequences formed the FSP probe complexes (lane 6). Notably, the FSP complex remained in a stable state in the presence of the fuel (lane 7). It further validated that the added target sequence induced D2 separation from the FSP probe (lane 8). Importantly, we confirmed that the fuel functioned as programmed in generating fuel-

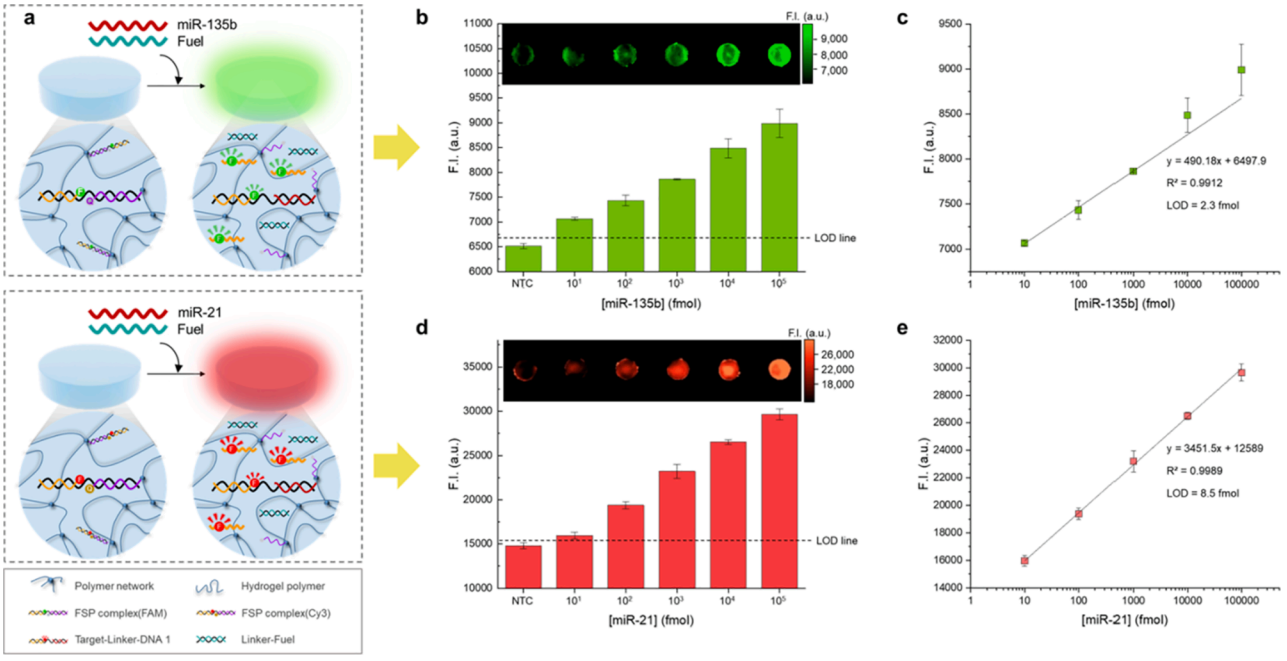

Fig. 2. Hydrogel-based fuel stimulant-powered (FSP) amplification for miRNA detection. a) Schematic illustration of FSP-hydrogel for the detection of miR-135b (green, top) and miR-21 (red, bottom). The FSP probe is immobilized in the hydrogel *via* photo-crosslinking. The target sequence and fuel initiate the FSP amplification reaction. b) Fluorescence images and intensities (F.I.) of cylindrical FSP-hydrogel in the presence of varying concentrations of synthetic miR-135b (10 fmol to 100 pmol). LOD, limit of detection (formula: 3 × standard deviation of linear regression (σ)/slope (m)). c) Calibration curve of FSP-135b-gel corresponding to the estimated detection limits. d) Fluorescence images and intensities of FSP probe specific for synthetic miR-21. e) Calibration curve of FSP-21-gel. The fluorescence intensities were assessed for triplicate sets ($n = 3$).

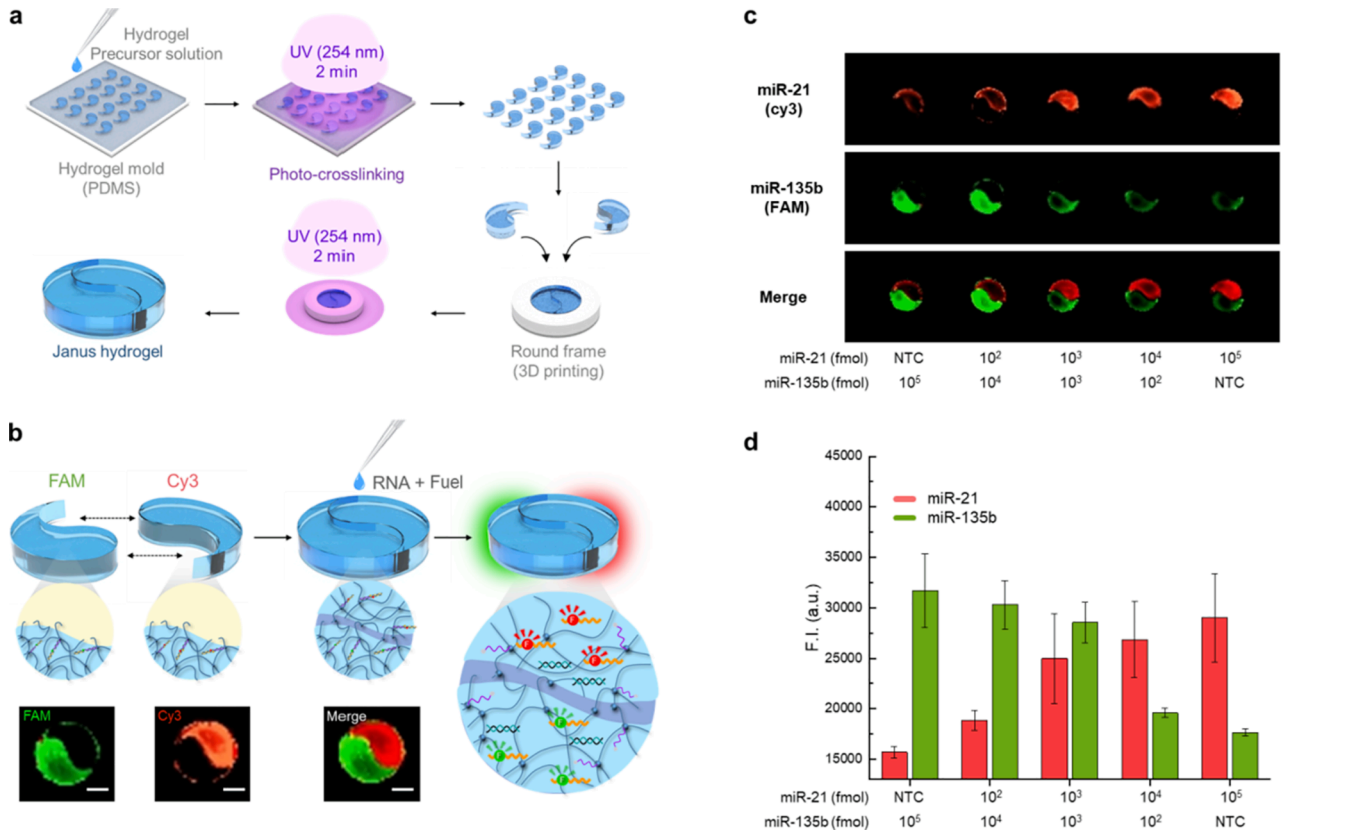

Fig. 3. Janus hydrogel-based fuel-stimulant-powered (FSP) amplification for simultaneous multiplex detection of miRNAs. a) Schematic illustration of the stepwise fabrication of a Janus hydrogel, consisting of two symmetric hydrogels. The hydrogels components are cured in a half-patterned hydrogel mold. Following photo-crosslinking by ultraviolet (UV) irradiation (254 nm, 2 min), two hydrogels are assembled in a round frame (3D printing). Each hydrogel is then combined *via* secondary UV irradiation (254 nm, 2 min). b) Schematic illustration of the Janus hydrogel-based FSP amplification for the detection of miR-135b and miR-21. One of the hydrogels in the pair is fluorescein phosphoramidite (FAM)-tagged FSP-135b, whereas the other is Cy3-tagged FSP-21 (Cy3). c) Fluorescence images of Janus FSP-hydrogel cross-treated with synthetic miRNAs (miR-21: increasing concentration from left to right; miR-135b: decreasing concentration from left to right; 100 fmol–100 pmol). d) Graphical representation of the fluorescence intensities visualized in (c). The fluorescence intensities represent that of sample triplicates ($n = 3$).

linker products and recycling the target sequence (lane 9).

Prior to validating the efficiency of FSP amplification, we first optimized the fuel concentration in an FSP probe-containing solution (**Figure S1**). In this regard, we prepared 100 nM of this solution with 100 nM (1:1), 500 nM (1:5), and 1 μM (1:10) of the fuel. Thereafter, we evaluated the real-time fluorescence intensities of the FSP probe for 2 h, both in the presence and absence of 1 nM of target sequence. At 100 nM and 500 nM of fuel concentrations, we observed that solution containing the target had 1.46- and 1.54-fold higher fluorescence intensities than no target control (NTC), respectively. However, NTC had increased fluorescence intensity at 1 μM fuel concentration, whereas the solution containing the target did not exhibit any increase in fluorescence intensity. In fact, we observed no significant increase in intensity despite adding high fuel concentrations to the solution; thus, we chose 100 nM (1:1 ratio) as the optimal fuel concentration. Next, we confirmed whether the fuel induced fluorescence signal amplification by evaluating the real-time fluorescence intensities of the FSP probes in the presence and absence of the fuel and 10 nM target for 2 h (Fig. 1d). In the absence of the fuel, no fluorescence signal amplification occurred even in the presence of the target. In contrast, fluorescence signal increased substantially in the presence of the fuel when compared to that in other conditions. To estimate the detection limits of FSP in solution, we measured the fluorescence intensities of the probes in the presence of varying concentrations of synthetic miRNAs (10 fmol to 100 pmol). **Figure S2** present the fluorescence intensities of the FSP-135b and FSP-21. Consequently, the following formula was used to calculate the limit of detection (LOD) = 3 × standard deviations of linear regression/slope; the detection limits of FSP-135b and FSP-21 were estimated to be 1.2 fmol and 1.1 fmol, respectively. Notably, the designed FSP probes exhibited high selectivity for the target (Fig. 1e). Additionally, we designed three control DNA sequences such that each of these sequences had a random single nucleotide changed from the target sequence. As shown in Fig. 1e, the fluorescence intensities of the FSP probes conjugated to the control DNA sequences hardly altered when compared to those of the FSP probes conjugated to the target.

3.2. Hydrogel-based FSP amplification for miRNA detection

A schematic illustration of cylindrical hydrogel synthesis is presented in **Figure S3**. We prepared a master template with vertical column patterns by 3D printing. Subsequently, we used this master template and polydimethylsiloxane (PDMS) to construct a hydrogel mold by soft lithography. We then poured a PDMS mixture containing a base and a curing agent (10:1 wt ratio) over the master template and heated it at 80 °C for 6 h. Once the PDMS layer was solidified, we peeled off the PDMS replica mold (*i.e.*, hydrogel mold) and placed it on a flat surface to expose its cylindrical cavities. Thereafter, a hydrogel precursor solution was poured in the hydrogel mold and cured with ultraviolet (UV) light irradiation (λ = 254 nm). The cured hydrogels were then collected from the mold and stored at 4℃ until further use.

Furthermore, we fabricated a hydrogel-based fuel stimulant by adding the FSP probe complex to the hydrogel precursor solution and curing it by UV irradiation. Before evaluating the performance of hydrogel-based FSP, we identified the optimal concentration of FSP probes required in the hydrogel to enhance detection sensitivity (**Figure S4**). In this regard, we prepared hydrogels containing 100 nM,

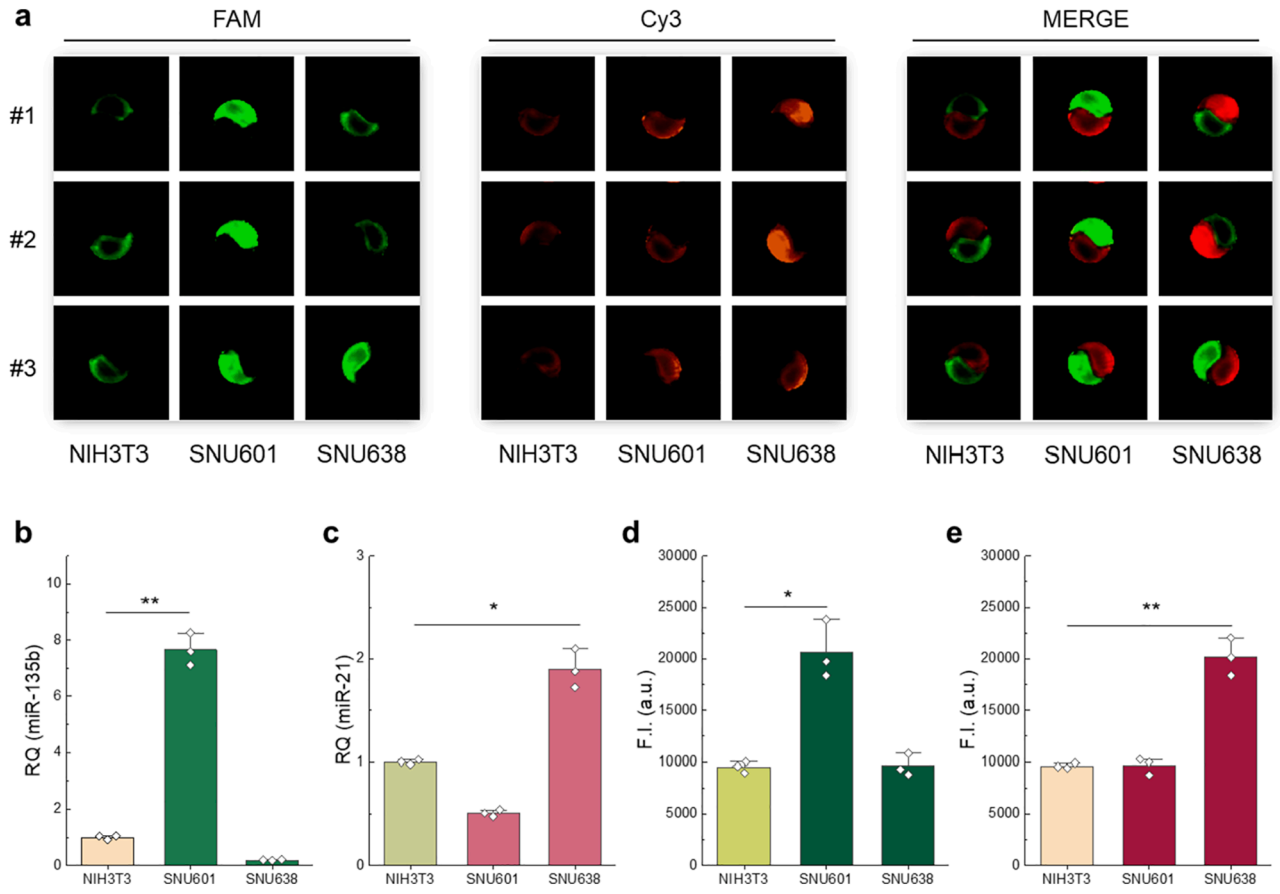

Fig. 4. *In vitro* performance of Janus hydrogel-based fuel stimulant-powered (FSP) amplification. a) Fluorescence images of simultaneous detection of two miRNAs in three different mammalian gastric cancer cell lines (NIH3T3, SNU601, and SNU638) using Janus FSP-hydrogel. b–c) Quantitative real-time PCR (qRT-PCR) analysis of (b) miR-135b and (c) miR-21 expression levels in the SNU601 and SNU638 gastric cancer cells compared to that in the NIH3T3 normal cells. Expression levels of these miRNAs were normalized to that of RNU6B. d–e) Fluorescence intensities in the (d) fluorescein phosphoramidite (FAM) region and (e) cyanine 3 (Cy3) region of the Janus hydrogel. These intensities indicate the detection of miR-135b (FAM) and miR-21 (Cy3) from the total RNA that is isolated from the cell cultured media ($n = 3$).

500 nM, and 1 μM FSP probes and added 1 nM of the target and 1:1 ratio of the fuel in each hydrogel. Consequently, the fluorescence intensities were 1.08, 1.48, and 1.19-fold higher in samples containing 100 nM, 500 nM, and 1 μM FSP probes, respectively, than that in NTC. Therefore, we conducted subsequent experiments using 500 nM FSP probes.

As shown in Fig. 2**a** we fabricated a two hydrogel-based FSP amplification process to detect cell-free miRNA markers of GC. To estimate the detection limits of the process, we measured the fluorescence intensities of the probes in the presence of varying concentrations of synthetic miRNAs (10 fmol to 100 pmol). Fig. 2b and d present the fluorescence intensities of the hydrogel-based FSP probes conjugated with miR-135b (FSP-135b-gel, green) and miR-21 (FSP-21-gel, red). We observed that the fluorescence intensity gradually increased with increase in the target sequence concentration. Consequently, we calculated the intensity to be linearly dependent on the logarithm (log) of the synthetic miRNA concentration (Fig. 2c, e). The linearly fitted equations were: $y = 490.18x + 6497.9$ ($R^2 = 0.9912$) and $y = 3451.5x + 12589$ ($R^2 = 0.9989$). Additionally, the following formula was used to calculate the limit of detection (LOD) = 3 × standard deviation of linear regression/slope; the detection limits of FSP-135b-gel and FSP-21-gel were estimated to be 2.3 fmol (46 pM) and 8.5 fmol (170 pM), respectively.

3.3. *Janus hydrogel-based FSP amplification for simultaneous multiplex miRNA detection*

To simultaneously detect miRNAs, we fabricated a yin-yang patterned Janus hydrogel by performing a UV-induced assembly of two symmetrical hydrogels (Fig. 3a). Indeed, the hydrogels were completely cured following UV irradiation for > 10 min (data not shown). Since curing starts from the upper surface of the hydrogel that faces the light, curing of the bottom and side of the hydrogel molds proceeds slowly [48,49]. However, when the surfaces of the two incompletely cured hydrogels are brought into contact with each other and are re-cured, the hydrogel polymer on the surfaces link, thereby assembling the two gels. We used the above method to manufacture hybrid hydrogels of various shapes and spatially divided patterns (**Figure S5**). In fact, we synthesized comma-shaped hydrogels (half of the Janus hydrogel) such that they could be perfectly combined into one hydrogel; this was performed by photolithography in the same manner as the development of cylindrical hydrogels. Once cured, each hydrogel was placed into a round frame and re-cured *via* UV irradiation (254 nm) for 2 min. Notably, half of the Janus hydrogel contained FSP-135b, whereas the other half contained FSP-21 (Fig. 3b).

Fig. 3c presents fluorescence images of a Janus hydrogel cross-treated with two synthetic miRNAs and the selective signal amplification of the target miRNAs. Fluorescence intensities of FSP-21-gel (red) and FSP-135b-gel (green) in mixed samples (increasing concentration of miR-21 from left to right and decreasing concentration of miR-135b from left to right) gradually increased or decreased with changes in the target sequence concentration (Fig. 3d). This indicated that the two different targets and fuels reacted independently.

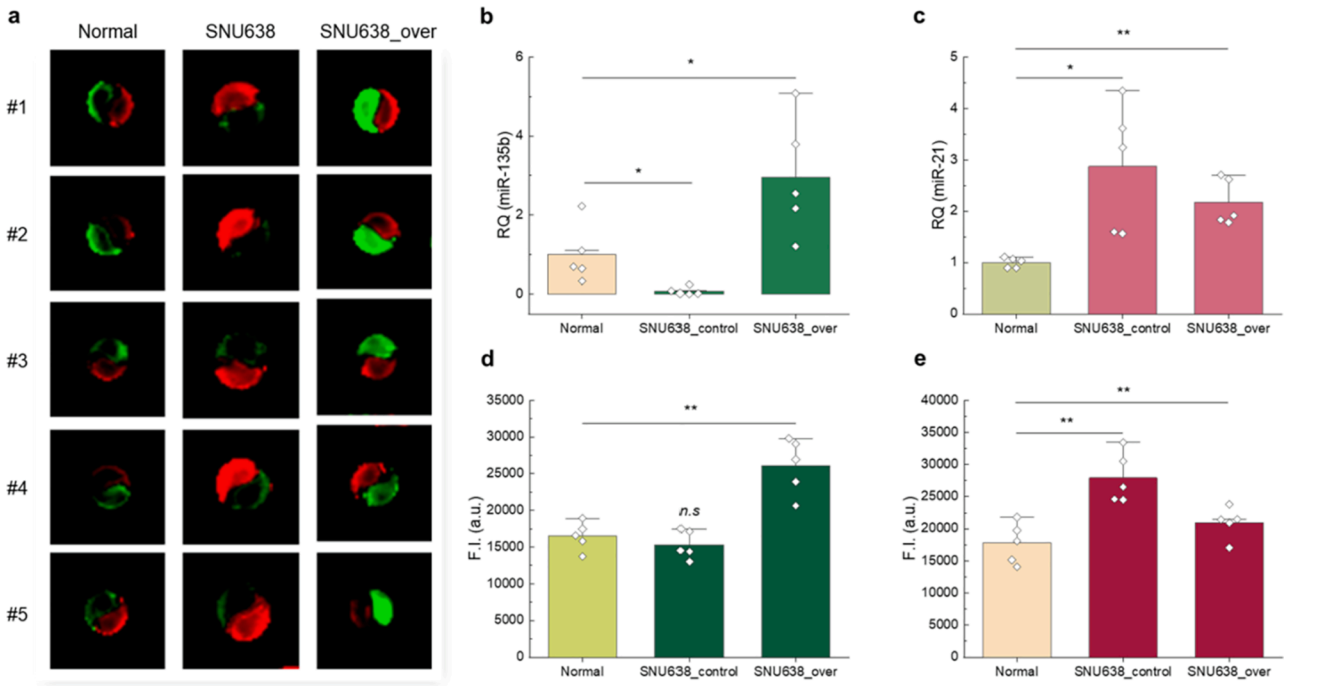

Fig. 5. *In vivo* performance of Janus hydrogel-based fuel stimulant-powered (FSP) amplification. a) Fluorescence images of Janus FSP-hydrogel with total RNA (100 ng of RNA/hydrogel) extracted from mice sera. The total RNA were isolated from the sera of three different mouse groups (Normal, SNU638_control, and SNU638_over). b–c) qRT-PCR analysis comparing the expression levels of (b) miR-135b and (c) miR-21 in mice sera. miRNA expression levels were normalized with that of RNU6B. d–e) Fluorescence intensities in the (d) fluorescein phosphoramidite (FAM) region and (e) and cyanine 3 (Cy3) region of the Janus hydrogel ($n = 5$). These intensities corresponded to miR-135b (FAM), and miR-21 (Cy3) expression levels among total RNA isolated from mice sera ($n = 5$).

3.4. Performance of Janus hydrogel-based FSP amplification in in vitro samples

First, we evaluated the expression levels of miR-135b and miR-21 in five different GC cell lines (SNU638, MKN-45, NCL-N87, KATO-III, and SNU601; **Figure S6**). Intriguingly, SNU638 had the lowest miR-135b expression among all the GC cell lines; however, it had the highest miR-21 expression. In contrast, SNU601 exhibited the highest miR-135b and the lowest miR-21 expression levels. Therefore, we selected these two cell lines to evaluate the *in vitro* performance of Janus hydrogels. Additionally, we compared the miRNA expression levels in these cells lines with those in normal cells (NIH3T3 mouse fibroblast cell line; **Figure S7**). Remarkably, SNU601 cells had 80-fold higher miR-135b expression and 0.5-fold lower miR-21 expression than NIH3T3 cells. However, SNU638 cells exhibited 0.05-fold lower miR-135b expression and 2.8-fold higher miR-21 expression than NIH3T3 cells.

Subsequently, we isolated total RNA from the cell culture media and treated the Janus hydrogels with 100 ng of this total RNA and obtained the resultant fluorescence images (Fig. 4a). However, we first assessed the expression levels of miR-135b and miR-21 by qRT-PCR (Fig. 4b and 4c). The expression patterns of miRNA extracted from the cell-cultured media are quite similar to that of miRNA extracted from cells. Remarkably, miR-135b exhibited the highest expression in SNU601 cells and the lowest expression in SNU638 cells. In contrast, miR-21 had the highest expression in SNU638 cells and the lowest expression in SNU601 cells. Fig. 4d depicts the expression of miR-135b (*i.e.*, green fluorescence of FAM) in the Janus hydrogel; SNU601 cells emitted more green fluorescence than NIH3T3 cells. In Fig. 4e, red fluorescence (Cy3) indicates the miR-21 expression in the Janus hydrogel; only SNU638 cells exhibited considerable increase in red fluorescence.

3.5. Performance of Janus hydrogel-based FSP amplification in in vivo samples

Next, we tested the performance of the Janus hydrogel in *in vivo* samples (Fig. 5a). In this regard, the in vivo samples comprised sera extracted from three mouse groups (normal, SNU638_control, and SNU638_over). First, we established an SNU638_135b overexpressing cell line (SNU638_over) by transfecting the pmR-ZsGreen1 vector (containing a full-length coding sequence of miR-135b) into cells. We then compared the miRNA expression levels in the miR-135b vector-transfected cell line with those in the parental SNU638 (normal) cells and SNU638_control (empty vector-transfected cells; **Figure S8**). Notably, miR-135b was upregulated by 35-folds in the SNU638_over cells compared to that in the parental cells (**Figure S8a**). Nonetheless, miR-21 expression had no significant differences between the three groups (**Figure S8b**). Furthermore, we established a xenograft mouse model *via* SNU638_control and SNU638_over cell injections. The tumor volumes were measured biweekly and estimated by the following formula: tumor volume = (length × width^2)/2 (**Figure S9**). Although we observed no difference in tumor sizes, miR-135b expression was relatively up-regulated in the SNU638_over tumor tissues compared to the SNU638_control (**Figure S10**). However, miR-21 was hardly altered. Remarkably, serum miR-135b levels were increased only in the SNU638_over group, concurring with our observation in the tumor tissue (Fig. 5b). In contrast, serum miR-21 levels were up-regulated in the SNU638_control and SNU638_over groups compared to that in the normal group (Fig. 5c). Consequently, we established an animal model suitable for testing the performance of the Janus hydrogel, while also analyzing serum miRNA expression levels to demonstrate the quantitative differences prevalent between the groups.

Efficiency of the Janus hydrogel in miRNA detection was tested in *in vivo* samples; the fluorescence intensities of the hydrogel were measured after 2 h of incubation at room temperature. The tested samples comprised 100 ng of miRNA extracted from mouse serum and 500 nM each of fuel-135b and fuel-21. Notably, the SNU638_control group exhibited lower fluorescence in the miR-135b (FAM) region of the Janus hydrogel than the normal group, whereas SNU638_over group exhibited the highest fluorescence in this region among all the in vivo groups (Fig. 5d). In contrast, both the xenograft mouse models had higher

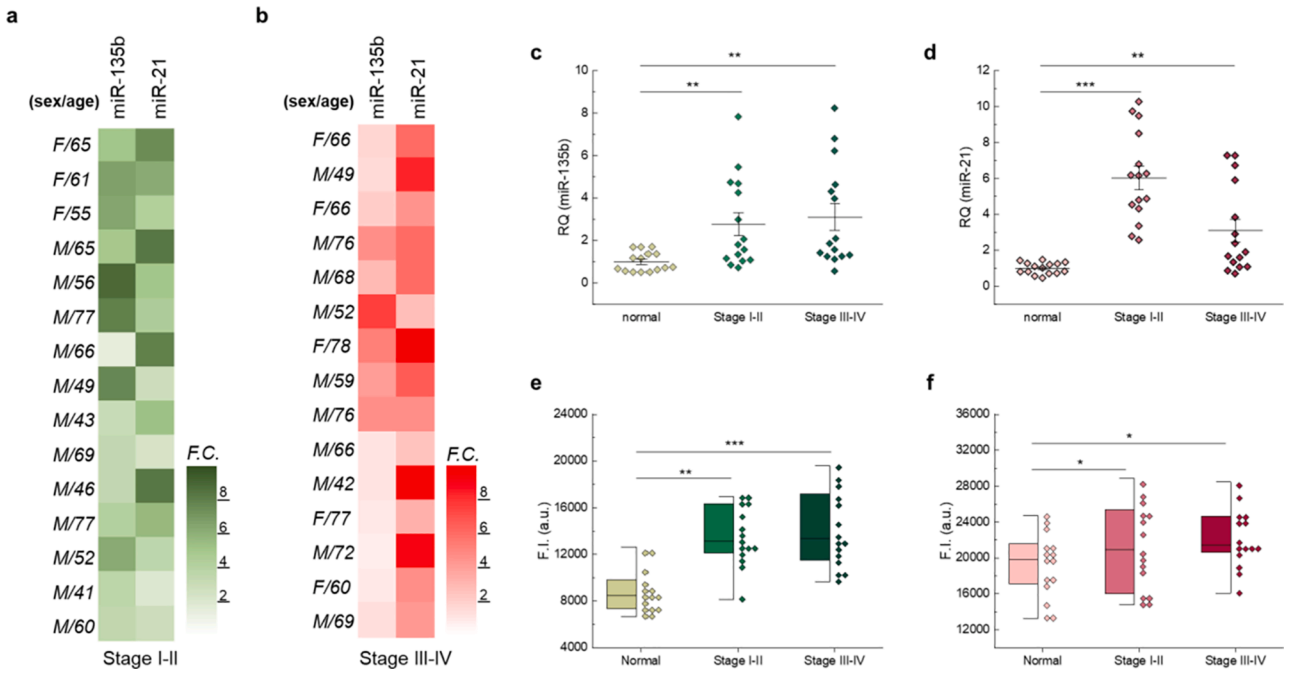

Fig. 6. Application of Janus hydrogel-based fuel stimulant-powered (FSP) amplification to human clinical samples. a–b) Heatmap of serum expression levels of miR-135b and miR-21 in (a) stage I–II and (b) stage III–IV gastric cancer patients compared to those in normal (healthy control) individuals (n = 15). c–d) qRT-PCR analysis of (c) miR-135b and (d) and miR-21 expression levels in patient sera. e–f) Fluorescence intensities corresponding to (e) miR-135b and (f) and miR-21 expression levels detected using Janus hydrogel in patient sera (n = 15).

fluorescence in the miR-21 region (Cy3) of the Janus hydrogel than the control group (Fig. 5e); this was consistent with our qRT-PCR data.

3.6. *Application of Janus hydrogel-based FSP amplification to human clinical samples*

We obtained human clinical serum samples from normal (healthy control) individuals and stages I–II and stages III–IV GC patients. Fig. 6a and 6b present heatmaps of miR-135b and miR-21 serum expression levels in stage I–II and stage III–IV GC patients, respectively. We validated *via* qRT-PCR that miR-135b and miR-21 expression levels were up-regulated in these patients than those in the healthy control (Fig. 6c–d).

Subsequently, we simultaneously detected miR-135b and miR-21 in the human serum samples by performing Janus hydrogel-based FSP amplification under optimized conditions. The evaluated fluorescence intensities revealed that miR-135b and miR-21 were up-regulated in the patients compared to that in the healthy controls (Fig. 6e–f). These results indicated that Janus hydrogel-based FSP amplification of human serum samples produced reliable fluorescent signals and is a potential clinical tool for GC diagnosis.

4. Conclusions

In this study, we propose a novel diagnostic platform comprising FSP probes in hydrogels. It enhances detection sensitivity *via* enzyme-free signal amplification in identifying circulating miRNAs. Here, we designed two FSP probes specific for the GC-associated miRNAs hsa-miR-135b and hsa-miR-21; we immobilized them in the hydrogel. The efficiency of these hydrogel-based FSP probes (FSP-135b-gel and FSP-21-gel) were validated by using synthetic targets. Indeed, their LOD were found to be 2.3 fmol and 8.5 fmol, respectively. Furthermore, we manufactured a yin-yang-patterned Janus hydrogel by assembling two symmetrically manufactured hydrogels for the simultaneous detection of miR-135b and miR-21 by either of the two hydrogels. The performance of the Janus hydrogel in detecting miRNAs extracted from cell culture medium, mouse sera, and human sera was compared to that of qRT-PCR. In fact, miRNAs extracted from the biological samples and analyzed by Janus hydrogel-based FSP amplification exhibited similar expression patterns as those analyzed by qRT-PCR results. Eventually, we verified that both the target miRNA were upregulated in the clinical samples. Thus, to the best of our knowledge, our results are the first of its kind on Janus hydrogel-based FSP amplification for gastric cancer-related miRNA detection.

Declaration of Competing Interest

The authors declare that they have no known competing financial interests or personal relationships that could have appeared to influence the work reported in this paper.

Acknowledgments

E. -K. Lim acknowledges support from the National R&D Programs through National Research Foundation (NRF) of Korea funded by Ministry of Science and ICT (MSIT) of Korea (NRF-2020R1A2C1010453, NRF-2021M3H4A1A02051048, NRF-2021M3E5E3080379, and NRF-2018M3A9E2022821), Technology Development Program for Biological Hazards Management in Indoor Air through Korea Environment Industry & Technology Institute (KEITI) funded by Ministry of Environment (ME) of Korea (2021003370003), K-Sensor Technology Development Program funded by Ministry of Trade, Industry, and Energy (MOTIE) of Korea (RS-2022-00154855), and KRIBB Research Initiative Program (1711134081). T.S. Han acknowledges support from the Korean Fund for Regenerative Medicine, a grant funded by the Korea government (the Ministry of Science and ICT, the Ministry of Health & Welfare, 21A0404L1), the NRF funded by the Ministry of Science and ICT (NRF-2020R1C1C1007431), and the KRIBB Research Initiative Program (1711170580).

Appendix A. Supplementary data

Supplementary data to this article can be found online at https://doi.

org/10.1016/j.cej.2022.137637.

References

[1] H. Sung, J. Ferlay, R.L. Siegel, M. Laversanne, I. Soerjomataram, A. Jemal, F. Bray, Global Cancer Statistics 2020: GLOBOCAN Estimates of Incidence and Mortality Worldwide for 36 Cancers in 185 Countries, CA Cancer J Clin 71 (2021) (2020) 209–249.

[2] M. Arnold, J.Y. Park, M.C. Camargo, N. Lunet, D. Forman, I. Soerjomataram, Is gastric cancer becoming a rare disease? A global assessment of predicted incidence trends to 2035, Gut 69 (5) (2020) 823–829.

[3] S. Emoto, H. Ishigami, H. Yamashita, H. Yamaguchi, S. Kaisaki, J. Kitayama, Clinical significance of CA125 and CA72-4 in gastric cancer with peritoneal dissemination, Gastric Cancer 15 (2) (2012) 154–161.

[4] A.R. Choi, J.C. Park, J.H. Kim, S.K. Shin, S.K. Lee, Y.C. Lee, J.B. Chung, High level of preoperative carbohydrate antigen 19–9 is a poor survival predictor in gastric cancer, World J Gastroenterol 19 (2013) 5302–5308.

[5] H. Shimada, T. Noie, M. Ohashi, K. Oba, Y. Takahashi, Clinical significance of serum tumor markers for gastric cancer: a systematic review of literature by the Task Force of the Japanese Gastric Cancer Association, Gastric Cancer 17 (2014) 26–33.

[6] B. Joypaul, M. Browning, E. Newman, D. Byrne, A. Cuschieri, Comparison of serum CA 72–4 and CA 19–9 levels in gastric cancer patients and correlation with recurrence, Am J Surg 169 (6) (1995) 595–599.

[7] M.M. Tsai, C.S. Wang, C.Y. Tsai, H.W. Huang, H.C. Chi, Y.H. Lin, P.H. Lu, K.H. Lin, Potential diagnostic, prognostic and therapeutic targets of MicroRNAs in human gastric cancer, Int J Mol Sci 17 (2016) 945.

[8] J.B.Y. So, R. Kapoor, F. Zhu, C. Koh, L. Zhou, R. Zou, Y.C. Tang, P.C.K. Goo, S. Y. Rha, H.C. Chung, J. Yoong, C.T. Yap, J. Rao, C.-K. Chia, S. Tsao, A. Shabbir, J. Lee, K.-P. Lam, M. Hartman, W.P. Yong, H.-P. Too, K.-G. Yeoh, Development and validation of a serum microRNA biomarker panel for detecting gastric cancer in a high-risk population, Gut 70 (5) (2021) 829–837.

[9] L. Necula, L. Matei, D. Dragu, A.I. Neagu, C. Mambet, S. Nedeianu, C. Bleotu, C. C. Diaconu, M. Chivu-Economescu, Recent advances in gastric cancer early diagnosis, World J Gastroenterol 25 (17) (2019) 2029–2044.

[10] M. Ha, V.N. Kim, Regulation of microRNA biogenesis, Nat Rev Mol Cell Biol 15 (8) (2014) 509–524.

[11] Y. Lee, C. Ahn, J. Han, H. Choi, J. Kim, J. Yim, J. Lee, P. Provost, O. Rådmark, S. Kim, V.N. Kim, The nuclear RNase III Drosha initiates microRNA processing, Nature 425 (6956) (2003) 415–419.

[12] D. Vasilatou, S. Papageorgiou, V. Pappa, E. Papageorgiou, J. Dervenoulas, The role of microRNAs in normal and malignant hematopoiesis, Eur J Haematol 84 (2010) 1–16.

[13] J. Lu, G. Getz, E.A. Miska, E. Alvarez-Saavedra, J. Lamb, D. Peck, A. Sweet-Cordero, B.L. Ebert, R.H. Mak, A.A. Ferrando, J.R. Downing, T. Jacks, H.R. Horvitz, T.R. Golub, MicroRNA expression profiles classify human cancers, Nature 435 (7043) (2005) 834–838.

[14] H. Ishiguro, M. Kimura, H. Takeyama, Role of microRNAs in gastric cancer, World J Gastroenterol 20 (2014) 5694–5699.

[15] R. Rupaimoole, F.J. Slack, MicroRNA therapeutics: towards a new era for the management of cancer and other diseases, Nat Rev Drug Discov 16 (2017) 203–222.

[16] Y.u. Li, K.V. Kowdley, MicroRNAs in common human diseases, Genomics Proteomics Bioinformatics 10 (5) (2012) 246–253.

[17] T.N. Patel, S. Roy, R. Ravi, Gastric cancer and related epigenetic alterations, Ecancermedicalscience 11 (2017) 714.

[18] S. Lin, R.I. Gregory, MicroRNA biogenesis pathways in cancer, Nat Rev Cancer 15 (6) (2015) 321–333.

[19] D. Kong, Y.-S. Piao, S. Yamashita, H. Oshima, K. Oguma, S. Fushida, T. Fujimura, T. Minamoto, H. Seno, Y. Yamada, K. Satou, T. Ushijima, T.-O. Ishikawa, M. Oshima, Inflammation-induced repression of tumor suppressor miR-7 in gastric tumor cells, Oncogene 31 (35) (2012) 3949–3960.

[20] E. Larrea, C. Sole, L. Manterola, I. Goicoechea, M. Armesto, M. Arestin, M. M. Caffarel, A.M. Araujo, M. Araiz, M. Fernandez-Mercado, C.H. Lawrie, New Concepts in Cancer Biomarkers: Circulating miRNAs in Liquid Biopsies, Int J Mol Sci 17 (2016) 627.

[21] N. Kosaka, H. Iguchi, T. Ochiya, Circulating microRNA in body fluid: a new potential biomarker for cancer diagnosis and prognosis, Cancer Sci 101 (2010) 2087–2092.

[22] A. Shiotani, T. Murao, Y. Kimura, H. Matsumoto, T. Kamada, H. Kusunoki, K. Inoue, N. Uedo, H. Iishi, K. Haruma, Identification of serum miRNAs as novel non-invasive biomarkers for detection of high risk for early gastric cancer, Br J Cancer 109 (9) (2013) 2323–2330.

[23] Q. Li, B. Li, Q. Li, S. Wei, Z. He, X. Huang, L. Wang, Y. Xia, Z. Xu, Z. Li, W. Wang, L. Yang, D. Zhang, Z. Xu, Exosomal miR-21-5p derived from gastric cancer promotes peritoneal metastasis via mesothelial-to-mesenchymal transition, Cell Death Dis 9 (2018) 854.

[24] H. Konishi, D. Ichikawa, S. Komatsu, A. Shiozaki, M. Tsujiura, H. Takeshita, R. Morimura, H. Nagata, T. Arita, T. Kawaguchi, S. Hirashima, H. Fujiwara, K. Okamoto, E. Otsuji, Detection of gastric cancer-associated microRNAs on microRNA microarray comparing pre- and post-operative plasma, Br J Cancer 106 (4) (2012) 740–747.

[25] C.-G. Liu, G.A. Calin, S. Volinia, C.M. Croce, MicroRNA expression profiling using microarrays, Nat Protoc 3 (4) (2008) 563–578.

[26] M. Sierzega, M. Kaczor, P. Kolodziejczyk, J. Kulig, M. Sanak, P. Richter, Evaluation of serum microRNA biomarkers for gastric cancer based on blood and tissue pools profiling: the importance of miR-21 and miR-331, Br J Cancer 117 (2017) 266–273.

[27] X. Zhou, W. Zhu, H. Li, W. Wen, W. Cheng, F. Wang, Y. Wu, L. Qi, Y. Fan, Y. Chen, Y. Ding, J. Xu, J. Qian, Z. Huang, T. Wang, D. Zhu, Y. Shu, P. Liu, Diagnostic value of a plasma microRNA signature in gastric cancer: a microRNA expression analysis, Sci Rep 5 (2015) 11251.

[28] A.A. Hardikar, R.J. Farr, M.V. Joglekar, Circulating microRNAs: understanding the limits for quantitative measurement by real-time PCR, J Am Heart Assoc 3 (2014) e000792.

[29] W. Tian, P. Li, W. He, C. Liu, Z. Li, Rolling circle extension-actuated loop-mediated isothermal amplification (RCA-LAMP) for ultrasensitive detection of microRNAs, Biosens Bioelectron 128 (2019) 17–22.

[30] A. Grundhoff, C.S. Sullivan, D. Ganem, A combined computational and microarray-based approach identifies novel microRNAs encoded by human gamma-herpesviruses, RNA 12 (5) (2006) 733–750.

[31] T. Kanagawa, Bias and artifacts in multitemplate polymerase chain reactions (PCR), J Biosci Bioeng 96 (2003) 317–323.

[32] P. Miao, Y. Tang, Cascade Strand Displacement and Bipedal Walking Based DNA Logic System for miRNA, ACS Cent Sci 7 (2021) 1036-1044.

[33] P. Miao, Y. Tang, Gold nanoparticles-based multipedal DNA walker for ratiometric detection of circulating tumor cell, Anal Chem 91 (23) (2019) 15187–15192.

[34] D.C. Pregibon, M. Toner, P.S. Doyle, Multifunctional encoded particles for high-throughput biomolecule analysis, Science 315 (5817) (2007) 1393–1396.

[35] J. Kim, J.S. Shim, B.H. Han, H.J. Kim, J. Park, I.J. Cho, S.G. Kang, J.Y. Kang, K. W. Bong, N. Choi, Hydrogel-based hybridization chain reaction (HCR) for detection of urinary exosomal miRNAs as a diagnostic tool of prostate cancer, Biosens Bioelectron 192 (2021), 113504.

[36] D.C. Appleyard, S.C. Chapin, R.L. Srinivas, P.S. Doyle, Bar-coded hydrogel microparticles for protein detection: synthesis, assay and scanning, Nat Protoc 6 (2011) 1761–1774.

[37] Y. Lee, W.J. Song, J.-Y. Sun, Hydrogel soft robotics, Materials Today Physics 15 (2020) 100258.

[38] X. He, T. Zeng, Z. Li, G. Wang, N. Ma, Catalytic Molecular Imaging of MicroRNA in Living Cells by DNA-Programmed Nanoparticle Disassembly, Angew Chem Int Ed Engl 55 (9) (2016) 3073–3076.

[39] V.A. Sontakke, Y. Yokobayashi, Programmable Macroscopic Self-Assembly of DNA-Decorated Hydrogels, J Am Chem Soc 144 (5) (2022) 2149–2155.

[40] T.-S. Han, D.-C. Voon, H. Oshima, M. Nakayama, K. Echizen, E. Sakai, Z.W.E. Yong, K. Murakami, L. Yu, T. Minamoto, C.-Y. Ock, B.J. Jenkins, S.-J. Kim, H.-K. Yang, M. Oshima, Interleukin 1 Up-regulates MicroRNA 135b to Promote Inflammation-Associated Gastric Carcinogenesis in Mice, Gastroenterology 156 (4) (2019) 1140–1155.e4.

[41] J. Wu, G. Li, Z. Wang, Y. Yao, R. Chen, X. Pu, J. Wang, Circulating MicroRNA-21 Is a Potential Diagnostic Biomarker in Gastric Cancer, Dis Markers 2015 (2015), 435656.

[42] J. Zheng, H. Xue, T. Wang, Y. Jiang, B. Liu, J. Li, Y. Liu, W. Wang, B. Zhang, M. Sun, miR-21 downregulates the tumor suppressor P12 CDK2AP1 and stimulates cell proliferation and invasion, J Cell Biochem 112 (3) (2011) 872–880.

[43] D. Sekar, R. Krishnan, K. Thirugnanasambantham, B. Rajasekaran, V.I.H. Islam, P. Sekar, Significance of microRNA 21 in gastric cancer, Clin Res Hepatol Gastroenterol 40 (5) (2016) 538–545.

[44] E.S. Martens-Uzunova, M. Olvedy, G. Jenster, Beyond microRNA–novel RNAs derived from small non-coding RNA and their implication in cancer, Cancer Lett 340 (2) (2013) 201–211.

[45] H. Kaija, L. Pakanen, K. Porvari, RNU6B, a frequent reference in miRNA expression studies, differentiates between deaths caused by hypothermia and chronic cardiac ischemia, Int J Legal Med 134 (1) (2020) 159–162.

[46] K.R. Stevens, J.S. Miller, B.L. Blakely, C.S. Chen, S.N. Bhatia, Degradable hydrogels derived from PEG-diacrylamide for hepatic tissue engineering, J Biomed Mater Res A 103 (10) (2015) 3331–3338.

[47] D.L. Elbert, J.A. Hubbell, Conjugate addition reactions combined with free-radical cross-linking for the design of materials for tissue engineering, Biomacromolecules 2 (2) (2001) 430–441.

[48] M. Madaghiele, L. Salvatore, C. Demitri, A. Sannino, Fast synthesis of poly (ethylene glycol) diacrylate cryogels via UV irradiation, Mater. Lett. 218 (2018) 305–308.

[49] W. Choi, S.Y. Yeom, J. Kim, S. Jung, S. Jung, T.S. Shim, S.K. Kim, J.Y. Kang, S. H. Lee, I.J. Cho, J. Choi, N. Choi, Hydrogel micropost-based qPCR for multiplex detection of miRNAs associated with Alzheimer's disease, Biosens Bioelectron 101 (2018) 235–244.